Analyses & Alternatives Vol. 10 No. 2. June 2026.
DOI: 10.22931/aanda.2026.10.2.001

Satellite Nighttime Lights and Urban Resilience under Sanctions: A North Korean Case

Dong Jun CHUN*
Korea Environment Institute
Jun-Kee BAEK**
Hanshin University

Abstract

International sanctions and pandemic-era border closures rarely affect cities evenly, yet within-country distributional effects remain difficult to measure when the targeted state publishes no reliable sub-national statistics. This paper addresses the gap using a relatively underused approach in Korean studies and political economy: a high-frequency satellite nighttime-lights (NTL) panel applied to North Korea. Drawing on NASA's daily Black Marble product over 2012–2025 for sixteen cities, the analysis detects 285 power-disruption (PD) and 577 flood-inducing rainfall (FL) events, then computes eight resilience metrics per event under a fixed pre-sanctions baseline. City fixed-effects regressions compare resilience across three regimes (pre-sanctions 2012–2015, post-sanctions 2017–2019, post-COVID 2020–2025); inference is reported conservatively via exact-enumeration wild cluster bootstrap (WCB) over all 2^4 = 16 sign patterns with G = 4 metropolitan clusters, alongside leave-one-cluster-out checks. Four findings emerge. First, a substantial capital-protection contrast in PD frequency: the Pyongyang-metropolitan cluster records 0.69 PD episodes per city-year against 2.49 in the east-inland cluster — a 3.6-fold rate gap that holds across alternative comparator schemes (illustratively, 17 events in the four most-protected core cities against 96 in the two most-exposed inland-border cities). Second, NTL responses to flood-inducing rainfall became

* First Author, Corresponding Author, Chief Reserch Fellow, Korea Environment Institute, E-mail: djchun@kei.re.kr
** Co-Author, Professor, College of Global Cooperation, Hanshin University, E-mail: misha99@hs.ac.kr

larger during the post-sanctions period (impact +0.109, scarring +0.188), consistent with — though without direct infrastructure observation of — weakened drainage or response capacity. Third, NTL impacts of both event types contract under post-COVID conditions (PD impact −0.061; FL impact −0.318), which the analysis interprets primarily as reduced measured urban activity rather than improved resilience. Fourth, an exploratory heterogeneous-treatment pattern (HC3-based, not validated under WCB) suggests that politically protected, low-exposure cities show larger post-COVID PD impacts than high-exposure cities (interaction +0.073), consistent with prior sanctions-era adaptation among the latter; this pattern warrants further investigation. The paper also illustrates how daily satellite NTL, when combined with transparent event definitions and panel-based robustness checks, can supplement conventional sources of evidence in opaque-state political-economy research.

Keywords
international sanctions, nighttime lights, North Korea, political geography, urban resilience

Analyses & Alternatives Vol. 10 No. 2. June 2026.
DOI: 10.22931/aanda.2026.10.2.001

위성 야간조도로 본 제재 국면 북한의 도시 회복탄력성: 16개 도시 사례

전동준*
한국환경연구원
백준기**
한신대학교

요약

국제제재와 팬데믹 시기의 국경봉쇄가 한 국가 안의 도시들에 미치는 영향은 결코 균등하지 않다. 그러나 제재 대상국이 신뢰할 만한 하위 행정구역 단위 통계를 공개하지 않는 한, 이러한 분배적 효과를 실증적으로 파악하기는 쉽지 않다. 본 연구는 한국학 및 정치경제 분야에서 그간 활용이 비교적 제한적이었던 고빈도 위성 야간조도(NTL: nighttime lights) 패널자료를 북한에 적용함으로써 이러한 실증적 공백을 메우고자 한다.

분석 대상은 북한의 16개 도시이며, NASA의 일별 Black Marble 산출물(2012–2025년)을 활용해 전력교란(PD: power-disruption) 285건과 홍수유발 강우(FL: flood-inducing rainfall) 577건의 사건을 식별한 뒤, 제재 이전 시기를 고정 기준선으로 한 8개 회복탄력성 지표를 사건별로 산출하였다. 세 시기—제재 이전(2012–2015년), 제재 강화 이후(2017–2019년), 코로나19 이후(2020–2025년)—간 회복탄력성의 차이는 도시 고정효과 회귀로 비교하였으며, 통계적 추론은 G = 4 광역도시 군집을 대상으로 $2^4 = 16$개 부호 조합을 완전 열거하는 와일드 군집 부트스트랩(WCB)과 군집별 1개 제외(leave-one-cluster-out) 검정을 병용하여 보수적으로 보고하였다.

분석 결과는 네 가지로 요약된다. 첫째, 전력교란 빈도 측면에서 ‘수도 보호 대비(capital-protection contrast)’가 뚜렷하게 확인된다. 평양 광역 군집의 도시·년 단위 연평균 발생률은 0.69건인 반면 동부 내륙 군집은 2.49건으로 약 3.6배에 달하는 격차가 나타나며, 이러한 패턴은 비교 도식을 달리해도 동일하게 유지된다(예컨대 보호 수준이 가장 높은 핵심 4개 도시는 13년간 17건, 노출이 가장 큰 내륙·접경 2개 도시는 96건). 둘째, 홍수유발 강우에 대한 NTL 반응은 제재 강화 이후 시기에 유의하게 확대되었다(impact 계수 +0.109, scarring

* 제1저자, 교신저자, 한국환경연구원 선임연구원, 이메일: djchun@kei.re.kr
** 공동저자, 한신대학교 글로벌 융합대학 교수, 이메일: misha99@hs.ac.kr

Analyses & Alternatives Vol. 10 No. 2. June 2026.
DOI: 10.22931/aanda.2026.10.2.001

계수 +0.188). 인프라를 직접 관측한 것은 아니지만, 이러한 결과는 배수 및 재난대응 역량의 약화와 부합하는 패턴으로 해석할 수 있다. 셋째, 코로나19 이후 시기에는 두 유형의 사건 모두 NTL 영향의 크기가 오히려 축소되는데(PD impact −0.061, FL impact −0.318), 본 연구는 이를 회복탄력성의 향상이 아니라 측정 가능한 도시 활동 수준 자체가 감소한 결과로 우선 해석한다. 넷째, 탐색적 수준에서 분석한 이질적 처치효과(HC3 표준오차 기반이며 WCB로는 검증되지 않음)에 따르면, 코로나19 이후 시기에 정치적 보호 수준이 높고 제재 노출이 낮은 도시일수록 PD 영향이 오히려 더 크게 나타나는 패턴(상호작용 계수 +0.073)이 관찰된다. 이는 노출이 큰 도시들이 제재 강화기에 이미 적응 과정을 거쳤다는 해석과 정합적이며, 후속 연구를 통한 정밀한 검증이 요구된다.
아울러 본 연구는 일별 위성 NTL 자료가 투명한 사건 식별 기준 및 패널 기반 강건성 검정과 결합될 때, 폐쇄성이 높은 국가의 정치경제 연구에서 전통적 자료원을 보완하는 유효한 증거자료로 기능할 수 있음을 함께 보여준다.

주제어
국제제재, 야간조도, 북한, 정치지리, 도시 회복탄력성

Ⅰ. Introduction

International sanctions are imposed on territories that are themselves internally uneven. A sanctions package targeting coal exports, textile manufacturing, or seafood does not affect a capital city dominated by political administration and a peripheral port that handles the targeted commodities in the same way. Yet the literature on sanctions effectiveness has typically measured outcomes at the national level — gross domestic product, trade volumes, regime concessions — leaving within-country distributional effects relatively underexplored (Drezner, 1999; Hufbauer et al., 2007; Peksen, 2009). The empirical difficulty is practical but binding: authoritarian states under sanctions publish limited or unreliable sub-national statistics, and cross-border household surveys typically reach only border populations.

This paper addresses the gap by introducing an alternative measurement strategy — daily satellite nighttime-lights (NTL) panel data — to the question of how international sanctions and the pandemic-era border closure differentially affected urban resilience across sixteen North Korean cities between 2012 and 2025. The analysis is positioned within the political-geography and political-economy traditions that engage closely with Korean studies scholarship, while drawing on a remote-sensing toolkit that has been less commonly used in this scholarly community. The paper therefore serves two purposes simultaneously: it produces substantive findings about the political geography of authoritarian urban resilience, and it illustrates how satellite-derived measures can supplement, rather than replace, conventional sources for opaque-state research.

Three findings stand out. First, a substantial capital-protection contrast between the Pyongyang-metropolitan core and inland-border periphery in PD frequency — a quantitative pattern that complements long-standing qualitative claims about preferential resource allocation in the North Korean political order (Lankov, 2013; Smith, 2015; Park Y., 2015). Second, NTL responses to flood-inducing rainfall events became larger during the post-sanctions period, a pattern consistent with weakened drainage or response capacity. Third, a counterintuitive heterogeneous-treatment-effect pattern under post-COVID conditions in which politically protected, low-exposure cities show larger power-disruption impacts than high-exposure border and industrial cities — a pattern that this paper interprets through an "adaptation under sanctions" mechanism. These findings extend the within-country distributional sanctions literature (Allen, 2008; Kim Byung-Yeon, 2017; Lee Suk, 2021) and the comparative authoritarian-urban-politics tradition (Slater, 2010; Wallace, 2014; Levitsky & Way, 2010) with replicable city-level satellite evidence without reliance on closed official statistics.

The remainder of the paper proceeds as follows. The literature review situates the analysis within sanctions, authoritarian-urban-politics, and satellite-NTL literatures. The data and methods section opens with a short *intuition box* introducing the NTL data type for readers unfamiliar with satellite-imagery analysis, followed by a *terminology box* defining the analytic vocabulary used throughout. The results section presents the empirical findings. The discussion section interprets the findings and addresses methodological caveats. The conclusion summarizes the findings and outlines policy implications.

Ⅱ. Literature Review and Theoretical Framing

1. Sanctions, Authoritarian Cities, and Selective State Capacity

Three literatures inform the analysis. First, the international-sanctions literature documents extensive aggregate effects on target-state economies (Hufbauer et al., 2007; Neuenkirch & Neumeier, 2015) and a sustained debate about whether sanctions alter target-state behavior (Drezner, 1999; Pape, 1997; Peksen, 2009). Within-country distributional work has emphasized elite-versus-mass impacts (Allen, 2008; Early, 2015) or household consumption effects under marketization (Kim Byung-Yeon, 2017). For North Korea specifically, Lee Suk (2021) provides the most comprehensive

Korean-language assessment of how UN sanctions from 2016–2017 affected trade, industry, foreign exchange, market activity, and food security; Yang Moon-Soo (2005) and Kim Byung-Ro (2012) document the formation and segmented character of North Korean markets since the late 1990s. Park Young-ja (2015) anchors the empirical study of cleavages and political-functional differentiation across North Korean cities. These Korean-language works form the substantive backdrop against which the present satellite-derived patterns are interpreted.

Second, the political-geography and authoritarian-urban-politics tradition argues that capital regions in non-democratic states enjoy preferential resource allocation through "protection pacts" (Slater, 2010) or "urban bias" (Wallace, 2014). Levitsky and Way (2010) formalize this with the "selective state capacity" concept: authoritarian regimes deliver public services unevenly, prioritizing cities of greater political importance. Qualitative evidence on North Korea — defector interviews, journalist reporting, and policy studies — is consistent with such a pattern, particularly for Pyongyang's preferential treatment in electricity, food supply, and infrastructure (Lankov, 2013; Smith, 2015; Min Kyung-Tae, 2014). Quantitative cross-city evidence has been lacking, and the present paper aims to provide such evidence at the resilience-dynamic level.

Third, the political economy of "natural" disasters and resilience identifies how governance configurations shape vulnerability to exogenous shocks (Cohen & Werker, 2008; Tierney, 2014; Meerow et al., 2016). The resilience-engineering framework of Bruneau et al. (2003) — robustness, redundancy, resourcefulness, and rapidity — was originally developed for seismic engineering applications and has since been adapted to socio-economic resilience contexts in disaster studies; the present paper operationalizes its dimensions on observable NTL trajectories.

2. Nighttime Lights as a Social-Science Method

Remote-sensing nighttime-lights data offer a relatively underused approach within Korean studies and political-economy research. Henderson, Storeygard, and Weil

(2012) established cross-country validation of NTL against gross domestic product where official statistics are weak; Hodler and Raschky (2014) used NTL to demonstrate regional favoritism patterns linked to political leadership. For sub-national or city-level analysis, newer VIIRS and Black Marble products (Elvidge et al., 2017; Román et al., 2018; Wang et al., 2021) provide daily, BRDF-corrected, gap-filled observations at fine spatial resolution.

North Korea has featured prominently in NTL-based work. Lee Yong Suk (2018) used DMSP-OLS data to document regional inequality dynamics under sanctions; Park Y. (2022) extended this with VIIRS data showing that incremental UN sanctions widened the Pyongyang–periphery luminosity gap (the Park 2022 source is a research brief and is cited as a directional benchmark rather than a fully peer-reviewed source). Event-detection applications of high-frequency NTL — used here to identify discrete power-disruption and flood-rainfall events rather than aggregate trends — emerged from Hurricane Maria and load-shedding studies (Elvidge et al., 2020; Román et al., 2019); the threshold settings used in this paper follow the conventions established in those works. The present paper extends this body by combining event-level dynamics with panel resilience metrics for a cross-city authoritarian-state setting.

3. Hypotheses

The analysis tests five substantive expectations; H4 is separated into occurrence and impact components. H1 is evaluated descriptively using event frequency and city-year-normalized event rates; H2 and H3 are evaluated with event-level fixed-effects regressions; H4a and H4b are evaluated descriptively and through the FL regression, respectively.

- **H1 (capital protection):** PD frequency in the Pyongyang-metropolitan cluster is significantly lower than in border and inland clusters because selective state capacity prioritizes the political core. - **H2 (sanctions exposure):** NTL responses to flood-inducing rainfall are larger in the post-sanctions period for high-exposure cities than for low-exposure cities, reflecting disproportionate weakening of drainage and emergency-response capacity in export-dependent industrial centers. – **H3 (COVID override through prior adaptation)**: Post-COVID PD impacts are smaller in absolute magnitude for high-exposure cities, which had already adapted to a lower economic-activity equilibrium during 2017–2019. – **H4a (rainfall occurrence is physical)**: Extreme rainfall occurrence is less politically clustered than PD episodes, because rainfall is a physical hazard. – **H4b (rainfall impact may still be political)**: NTL responses to extreme rainfall may vary across cities if drainage, infrastructure maintenance, and recovery capacity are politically uneven.

III. Data and Methods

The description below targets a social-science readership. Algorithmic specifications (quality-control flags, baseline alternatives, the eight resilience metrics, and the full inferential battery) are summarized in the supplementary materials. To support the computational workload of this study, the authors used Claude Code (Anthropic, Opus 4.7) to assist with code authoring (data ingestion, event-detection pipelines, panel-regression scripts) and with portions of the data analysis workflow; all analytical decisions, parameter choices, and final outputs were verified by the authors against the source data.

<Box 1> What Nighttime Lights Data Measure

The Visible Infrared Imaging Radiometer Suite (VIIRS) instrument aboard the Suomi National Polar-orbiting Partnership (Suomi-NPP) satellite passes over the Korean Peninsula every night and records the upwelling visible-band radiance from the Earth's surface, including the light emitted by electric lighting (street lamps, vehicle headlights, factory and commercial lighting, residential interior lighting visible through windows). NASA's Black Marble VNP46A2 product (Román et al., 2018) processes these nightly observations into a quality-controlled, calibrated

raster at approximately 500-meter spatial resolution, with corrections for moonlight, atmospheric scattering, snow, and stray light. Each pixel value is a radiance figure in $nW \cdot cm^{-2} \cdot sr^{-1}$ (a small physical unit of light brightness per area per solid angle); higher values indicate brighter pixels.

The conceptual link to social-science applications is straightforward. Where official statistics on sub-national economic activity, electricity supply, or infrastructure performance are absent or unreliable, the brightness of a city at night provides an observable, replicable proxy for urban human activity. A persistent and spatially coherent drop in nighttime brightness is consistent with reduced electricity supply, slowed industrial operation, decreased transport, or curtailed commercial activity. This approach does not identify the exact cause of the decline. Instead, it treats the decline as a measurable signal of urban functional disruption, whose subsequent return toward the pre-event level can be tracked as a recovery trajectory.

<Box 2> Key Terms Used in This Paper

Term	Meaning in this study
NTL	Satellite-observed nighttime radiance, used as a proxy for urban activity
PD episode	NTL-detected *power-disruption* episode (a city-specific NTL drop with spatial coherence and a rural-control-ring excess) — *not* a confirmed grid outage
FL event	*Flood-inducing rainfall* event (rainfall exceeding the city-specific 99th percentile, with terrain-risk conditions met) — *not* a confirmed inundation
Control ring	A 20–30 km rural annulus around a city's urban core, used to distinguish urban-specific NTL drops from regional artifacts
Impact depth	Relative size of the NTL decline at the event trough
Scarring	Mean residual deviation from the pre-event baseline over post-event weeks 8–16

1. Study Setting and Cities

The sample consists of sixteen North Korean cities selected to span four political-geographic dimensions (Figure 1, Table 1). The cities cover the political-administrative core (Pyongyang, Pyongsong), Sino-DPRK border-trade hubs (Sinuiju, Hyesan), east-coast heavy-industry ports (Chongjin, Hamhung, Kimchaek), an east-coast development node (Wonsan), special-economic-zone and DMZ-adjacent border cities (Rason, Kaesong), and Pyongyang-adjacent chemical-industrial centers and port (Sunchon, Anju, Nampo), with inland comparison cities (Sariwon, Kanggye) and a West-Sea provincial capital (Haeju). A seventeenth candidate, Tanchon, was screened but excluded because its nighttime-light extent and within-area-of-interest data-valid ratio fell below thresholds required for minimal reliability. To capture differential exposure to sanctions, cities are classified into three intensity categories: high (CHJ, HMH, KMC, SNU, HYS, KNG, RSN), medium (NMP, WNS, SCN, ANJ), and low (PYG, PSG, KSG, HAJ, SRW). Separately from exposure, cities are grouped into four metropolitan clusters for standard error estimation: Pyongyang-metro, east-coast, west-coast, and east-inland. The qualitative profiles of these cities — the politically protected character of Pyongsong, the chemical-industrial role of Anju and Sunchon, the military-industrial complex of Kanggye, the special-economic-zone status of Rason — draw on Park Young-ja (2015) and Min Kyung-Tae (2014).

<Figure 1> Study area and visualized analytical framework — (a) sixteen study cities on a GADM-clipped basemap; (b) representative NTL imagery contrasting Pyongyang and Kanggye baselines; (c) analytical workflow from input to output

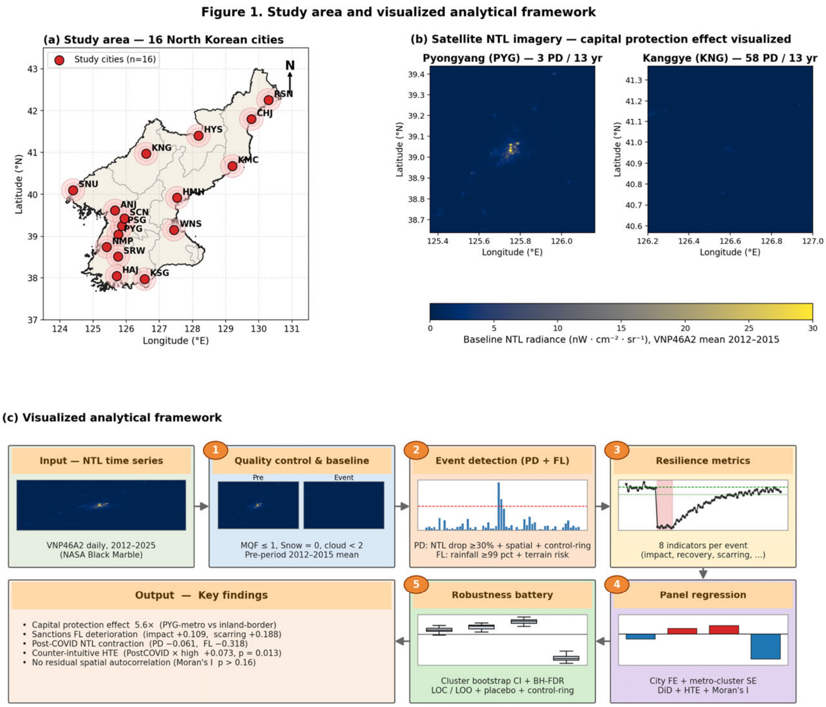

Source: Authors' construction from GADM v4.1 boundaries (panel a), NASA Black Marble VNP46A2 V002 (panel b), and analysis design (panel c).

The temporal scope (2012–2025) brackets three substantively distinct regimes: a pre-sanctions baseline (2012–2015), the post-sanctions period following UNSCR 2371, 2375, and 2397 (2017–2019), and the post-COVID border-closure period (2020–2025). The year 2016 is treated as a transition and excluded from period dummies.

<Table 1> Sixteen study cities—political-geographic attributes, sanctions-exposure intensity, and metropolitan cluster

Code	City	Coord (°N, °E)	Attributes	Intensity	Metro cluster
PYG	Pyongyang	39.04, 125.76	Core (capital)	Low	Pyongyang-metro
PSG	Pyongsong	39.25, 125.87	Capital satellite (science)	Low	Pyongyang-metro
NMP	Nampo	38.74, 125.41	Port, industrial	Med	Pyongyang-metro
SCN	Sunchon	39.43, 125.95	Industrial (chemical)	Med	Pyongyang-metro
ANJ	Anju	39.62, 125.66	Industrial (chemical/coal)	Med	Pyongyang-metro
SRW	Sariwon	38.51, 125.76	Inland (admin/agric.)	Low	Pyongyang-metro
KSG	Kaesong	37.97, 126.55	DMZ-adjacent border	Low	West-coast
SNU	Sinuiju	40.10, 124.40	Sino-border trade	High	West-coast
HAJ	Haeju	38.04, 125.72	Provincial seat, port	Low	West-coast
HMH	Hamhung	39.92, 127.54	Industrial (chemical)	High	East-coast
WNS	Wonsan	39.15, 127.44	East-coast port	Med	East-coast
CHJ	Chongjin	41.80, 129.78	Industrial port (steel)	High	East-coast
KMC	Kimchaek	40.67, 129.21	Industrial port (steel)	High	East-coast
HYS	Hyesan	41.40, 128.18	Border, mountain inland	High	East-inland
RSN	Rason	42.26, 130.30	Special economic zone	High	East-inland
KNG	Kanggye	40.97, 126.60	Provincial seat, military-industrial	High	East-inland

Source: Authors' construction. Intensity reflects the directness of city-level exposure to the export sectors targeted by UN sanctions (UNSCR 2371, 2375, 2397). Functional profiles draw on Park Young-ja (2015) and Min Kyung-Tae (2014).

2. Data and Event Detection

The analysis combines five sources. Daily nighttime-light radiance values come from NASA's Black Marble VNP46A2 V002 product (Román et al., 2018; Wang et al., 2021), filtered for cloud, snow, and lunar contamination. Daily rainfall comes from

CHIRPS v2.0 (Funk et al., 2015) sampled over a twenty-kilometer radius around each city. Terrain (elevation, slope) is derived from the Shuttle Radar Topography Mission (NASA JPL, 2013), administrative boundaries from the GADM project (GADM, 2022), and infrastructure (roads, waterways) from OpenStreetMap via Geofabrik (Geofabrik, 2024). For each city, five area-of-interest masks are constructed; analyses use the NTL-urban mask (lit-pixel core within thirty-kilometer buffer, clipped at the international border) for power-disruption analysis and the twenty-kilometer buffer for flood-rainfall analysis. Border clipping is an analytically essential step for any cross-border city study: Sinuiju's thirty-kilometer buffer drops from 5,206 to 1,340 lit pixels once Chinese-side light from Dandong is removed.

Daily NTL availability is uneven across cities and seasons because cloud cover, lunar illumination, and snow trigger quality-flag exclusions. Figure 2 shows the city-by-month count of valid VNP46A2 observation days across 2012–2025. Valid-observation density is highest from spring through autumn and lowest in mid-winter; mountainous border cities (HYS, RSN, KNG) record the lowest valid-day counts year-round. The pre-period (2012–2015) valid-observation ratios used for baseline construction range from 34.6 percent (KNG) to 55.8 percent (SNU), with all sixteen cities meeting a minimum reliability threshold defined before model estimation. Event-detection thresholds are calibrated per city to accommodate this heterogeneity. The asymmetry between the high-FL-risk season (summer, high data availability) and the high-PD-risk season (winter, lower data availability) is an inherent feature of the data environment rather than a methodological choice (see Limitations).

<Figure 2> City-by-month count of valid VNP46A2 nighttime-light observation days, 2012–2025

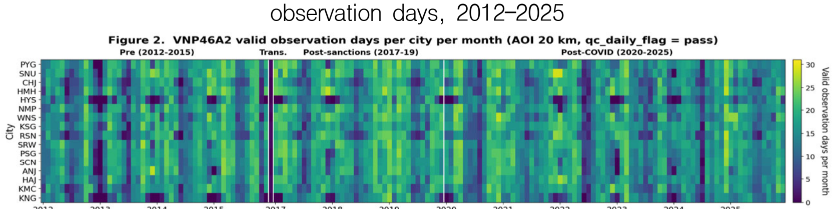

Source: Authors' construction from NASA Black Marble VNP46A2 V002 daily product after quality-control filtering (MQF ≤ 1, Snow = 0, cloud-confidence < 2).

A PD episode is identified when three conditions co-occur over consecutive days: an aggregate NTL drop of at least 30 percent relative to the 2012–2015 baseline, at least 60 percent of valid urban pixels showing pixel-level anomalies of comparable magnitude, and a city-versus-rural-control-ring difference of at least 0.10. These thresholds follow the conventions of Román et al. (2019) and Elvidge et al. (2020), adapted to the Korean context. An FL event begins when daily or three-day rolling rainfall exceeds the city-specific 99th-percentile threshold and the city's twenty-kilometer area-of-interest satisfies at least two of three terrain-risk flags (low-elevation ratio, gentle slope, near-water access). Three cities (HYS, SCN, KNG) fail the terrain filter and are pre-specified as excluded from flood analysis. Following Román et al. (2019) and Elvidge et al. (2020), these are framed as NTL-detected disruptions and rainfall-induced flood-risk events rather than as direct observations of grid outages or inundation, since ground-truth data are unavailable for North Korea.

Across sixteen cities and thirteen years (excluding 2016), the procedure identifies 285 PD episodes, 577 FL events, and 53 compound co-occurrences within ±2 weeks. Compound events are analyzed separately to avoid contamination of the pure-PD and pure-FL samples. The regression tables therefore use slightly different sample sizes from the raw event counts. Of the 285 PD episodes, 273 yield a QC-passing resilience-metric observation (event-metric observations) and enter the PD regressions. For FL, 582 event-metric observations enter the regressions — five more than the 577 raw FL episodes because a small number of long-duration rainfall events were split into adjacent recovery windows at the metric-computation stage and therefore contribute two metric rows each. All tables below report the regression unit of analysis explicitly.

3. Resilience Metrics and Identification

For each event, eight weekly-NTL resilience metrics are computed under a fixed pre-sanctions baseline. Figure 3 labels each metric on a stylized PD recovery curve so that social-science readers can see at a glance how the metrics relate to the underlying signal: impact depth, time-to-trough, trough value, recovery time to 90 % and to 95 % of baseline, post-trough recovery slope, scarring over post-event weeks 8–16, and post-event volatility. An additional area-under-the-curve loss summarizes the total deficit accumulated over the 16-week recovery window. Two alternative baselines (moving-window 60-day and week-of-year) are also computed; results are directionally similar but attenuated under adaptive baselines, an attenuation discussed in the *Activity-Effect Confound* subsection below.

<Figure 3> Eight resilience metrics on a stylized PD recovery curve

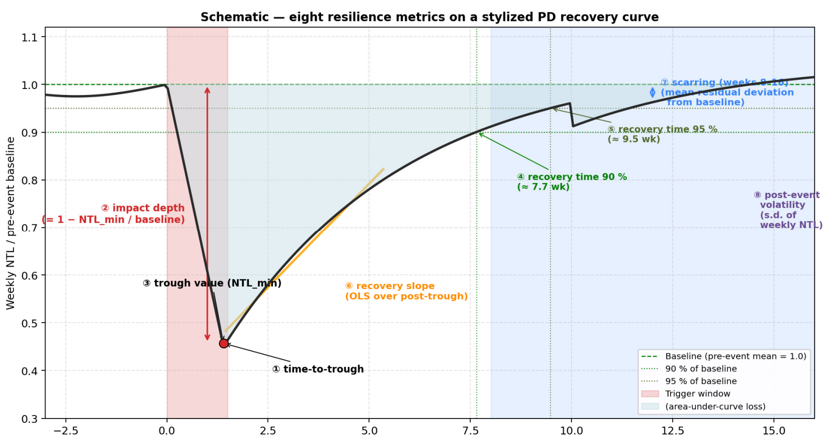

Source: Authors' construction. The eight metrics are labeled on a stylized weekly-NTL trajectory normalized to the pre-event baseline (= 1.0). Trigger window is shaded red; the 90 % and 95 % recovery thresholds are dashed green lines.

The estimating equation, applied to each resilience metric y and event e in city *i*, is

$$y_{i,e} = \alpha_i + \beta_1 \cdot \mathrm{PostSanctions}_e + \beta_2 \cdot \mathrm{PostCOVID}_e + \varepsilon_{i,e}$$

where the **city fixed effects** α_i absorb all time-invariant heterogeneity across cities (latitude, baseline industrial mix, distance to borders, terrain), and the period dummies are coded relative to the 2012–2015 reference. β_1 and β_2 measure the within-city change in resilience between regimes, holding constant city-level attributes; they do not, however, isolate the causal effect of sanctions or COVID from other co-occurring time-varying factors. The analysis therefore frames these coefficients as observational period contrasts rather than as quasi-experimental causal estimates.

Inference with a small number of clusters. Heteroskedasticity-consistent standard errors and metropolitan-cluster-robust standard errors are reported, alongside *exact-enumeration wild cluster bootstrap* (WCB) p-values (Cameron, Gelbach & Miller, 2008) for the four main outcomes. Because the number of metropolitan clusters is small (G = 4), conventional cluster-robust p-values can be unreliable; the WCB with Rademacher weights resampled at the cluster level provides an asymptotic refinement appropriate for small-G settings. With G = 4 there are exactly 2^4 = 16 unique sign patterns, so the analysis enumerates all 16 rather than random-sampling, yielding exact bootstrap p-values whose attainable floor is 1/16 ≈ 0.063 (when |t-statistic of original sample| exceeds the absolute value of every enumerated bootstrap t-statistic, the count is 0 and the reported p-value is approximately 0). The analysis emphasizes coefficient direction, magnitude, bootstrap intervals, and leave-one-unit-out robustness rather than p-values alone.

Heterogeneous treatment effects. A specification adds interactions of period dummies with the treatment-intensity category (low/medium/high), testing H2 and H3.

Robustness. Leave-one-cluster-out (LOC) and leave-one-city-out (LOO) re-estimations test sensitivity to influential units; Moran's I on residuals (with inverse-distance weights and 999 permutations) tests for residual spatial autocorrelation; an event-study specification estimates event-time-by-period coefficients to assess pre-trend behavior; a placebo test compares real-event resilience metrics against metrics computed on random non-event windows; and a control-ring test verifies that detected events represent urban-specific rather than regional phenomena. Analyses are implemented in Python 3.12 using statsmodels (Seabold & Perktold, 2010), with geospatial preprocessing via rasterio (Gillies, 2013–present), geopandas (Jordahl et al., 2020), and xarray (Hoyer & Hamman, 2017).

IV. Results

1. Event Frequencies and the Capital Protection Contrast

Across sixteen cities and thirteen analysis years, 285 PD episodes and 577 FL events are detected. The PD distribution exhibits the strongest political-geographic asymmetry observed in the analysis. The Pyongyang-metropolitan cluster (six cities including Pyongyang and its satellites) accounts for only 54 PD episodes — 18.9 percent of the total — and the west-coast cluster (three cities including Sinuiju and Kaesong) for 25 episodes (8.8 percent), whereas the east-inland cluster (three cities) contributes 97 episodes (34.0 percent) and the east-coast cluster (four cities) contributes 109 episodes (38.2 percent). Normalizing by cluster size makes the contrast still clearer (Table 2): the Pyongyang-metro cluster averages **0.69 PD episodes per city-year,** the west-coast cluster 0.64, the east-coast cluster 2.10, and the east-inland cluster 2.49 — a 3.6-fold gap between Pyongyang-metro and east-inland.

<Table 2> PD-event rate by metropolitan cluster, normalized by city-years

Cluster	Cities	PD events	City-years	PD per city-year	Share of total (%)
East-inland (HYS, RSN, KNG)	3	97	39	**2.49**	34.0
East-coast (HMH, WNS, CHJ, KMC)	4	109	52	**2.10**	38.2
Pyongyang-metro (PYG, PSG, NMP, SCN, ANJ, SRW)	6	54	78	**0.69**	18.9
West-coast (SNU, KSG, HAJ)	3	25	39	**0.64**	8.8

Source: Authors' construction. City-years are cities × 13 analysis years (2012–2025 excluding 2016).

As an illustrative contrast, the four most-protected Pyongyang-core cities (PYG, PSG, SCN, ANJ) record 17 PD episodes against 96 in the two most-exposed inland-border cities (KNG, RSN) — a five-to-six-fold gap in raw counts, which becomes roughly eleven-fold when expressed as rates per city-year. The broader cluster comparison in Table 2 points in the same direction. The pattern is not driven by NTL signal strength alone: Pyongsong (PSG), the second-most luminous city in the sample (1,835 lit pixels), records only one PD episode in thirteen years, whereas Kanggye (KNG), an inland militarized-industrial city with a much smaller lit-pixel count (206), records 58. The combination is best characterized as a capital-protection contrast. This contrast is illustrative rather than definitive — comparator choice matters, and the broader cluster-level pattern provides the more robust evidentiary basis.

FL frequencies show no comparable clustering: each FL-eligible city contributes 39–46 events with similar pre-sanctions, post-sanctions, and post-COVID proportions, supporting H4a — extreme rainfall *occurrence* is less politically clustered than PD episodes. The event calendar (Figure 4) makes both patterns visible.

<Figure 4> Event calendar — PD, FL, and compound events across 2012–2025

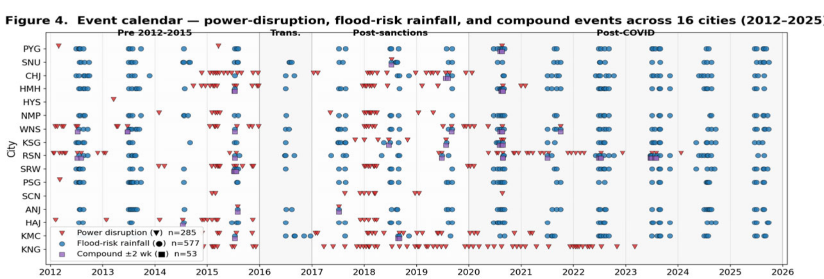

Source: Authors' construction. The 2016 transition year (excluded from period dummies) appears between the pre-sanctions and post-sanctions blocks.

2. Detection Validity

Two pre-specified validity tests indicate that the detected PD episodes reflect city-specific signals rather than random noise. In a *placebo test,* 302 random non-event windows of duration matched to the actual PD distribution (drawn from the same cities in non-event weeks) show median impact depth of 0.169 versus 0.495 for real events (Mann–Whitney *U*, $p < 0.001$) and median scarring of −0.159 versus 0.025 ($p < 0.001$). In a *control–ring test* — comparing each event's city area of interest with its 20–30 km rural annulus excluding lit pixels — the urban core shows a deeper impact than its rural surroundings in 72.9 percent of paired observations (Wilcoxon signed–rank, $p < 0.001$) and larger scarring in 83.2 percent ($p < 0.001$). These tests do not prove that every detected PD episode corresponds to a confirmed grid outage. They do, however, show that the detected events are not ordinary within–city fluctuations and are not simply regional artifacts shared by surrounding rural areas. The placebo gap (~0.33 in impact depth) is comparable to or exceeds magnitudes reported in Román et al. (2019) and Elvidge et al. (2020) for power–disruption NTL analyses elsewhere.

3. Within–City Regression Across Regimes

Table 3 reports the main fixed–effects regression results under the preferred specification (fixed pre–sanctions baseline) with three p–value columns side by side: heteroskedasticity–consistent (HC3), metropolitan–cluster–robust (G = 4), and exact–enumeration wild cluster bootstrap p–values over all $2^4 = 16$ Rademacher sign patterns.

<Table 3> City fixed–effects regression of resilience metrics on period dummies, with three p–value reports (sixteen cities)

Outcome	Term	β	(SE_metro)	p (HC3)	p (CRSE, G=4)	p (WCB enum)
PD impact (depth)	PostSanctions	−0.030	(0.023)	0.088	0.20	0.375
PD impact (depth)	PostCOVID	**−0.061**	(0.011)	0.006	<0.001	0.063
PD scarring (8–16 wk)	PostSanctions	**+0.072**	(0.012)	0.010	<0.001	**<0.063 (0/16)**
PD scarring (8–16 wk)	PostCOVID	+0.043	(0.047)	0.26	0.36	0.563

FL impact (depth)	PostSanctions	**+0.109**	(0.039)	0.001	0.005	0.063
FL impact (depth)	PostCOVID	**−0.318**	(0.064)	<0.001	<0.001	0.188
FL scarring (8–16 wk)	PostSanctions	**+0.188**	(0.043)	<0.001	<0.001	0.063
FL scarring (8–16 wk)	PostCOVID	**−0.345**	(0.037)	<0.001	<0.001	0.063

Note: Pre-sanctions period (2012–2015) is the reference category. City fixed effects are included. WCB enum = exact enumeration over all 2^4 = 16 Rademacher sign patterns at the metropolitan-cluster level (restricted-residual scheme); reported p-values are the fraction of the 16 enumerated patterns whose bootstrap-t statistic has absolute value greater than or equal to the original sample t-statistic. The attainable floor is 1/16 ≈ 0.063 (when the original t-statistic exceeds all 16 enumerated bootstrap t-statistics, the count is 0 and the p-value is reported as <0.063). PD scarring × PostSanctions reaches this case (0 of 16 patterns), indicating regime contrasts as statistically significant as the dataset's metropolitan geography permits. Source: Authors' computations.

Five points are worth emphasizing.

First, **PD scarring under post-sanctions** rises by 0.072 (HC3 $p = 0.010$), with all 16 enumerated WCB sign patterns producing smaller |t|-statistics than the original (WCB $p < 0.063$, the floor). This is the most strongly statistically supported finding in the table. PD events during 2017–2019 left more persistent post-event NTL deficits than pre-sanctions-period events, an erosion observed during the post-sanctions period that is consistent with — though without direct infrastructure observation of — reduced redundancy in supply chains, fuel stocks, and equipment-replacement capacity (Bruneau et al., 2003; Tierney, 2014).

Second, **the post-COVID PD impact contraction** of −0.061 (HC3 $p = 0.006$) has WCB $p = 0.063$, exactly the floor permitted by the four-cluster sample size. Given that the minimum attainable p-value under a four-cluster wild bootstrap is approximately 0.063, observing p-values at this mathematical floor indicates the regime contrasts are as statistically significant as the dataset's metropolitan geography permits. The direction is stable in leave-one-cluster-out checks.

Third, **NTL responses to flood-inducing rainfall** become larger under post-sanctions (impact +0.109; scarring +0.188) and smaller (more negative) under post-COVID (impact −0.318; scarring −0.345). HC3 and conventional CRSE indicate $p < 0.01$ for all four FL coefficients; WCB returns the four-cluster floor for three of the four ($p \approx 0.063$) and 0.188 for FL impact × PostCOVID. The direction is stable in LOC and LOO checks; conservative WCB inference indicates that statistical certainty is limited by the small number of metropolitan clusters rather than by coefficient size. NTL contractions reported here should be read as a composite of two mechanisms: (i) shifts in resilience or response capacity at the event level, and (ii) reductions in measured baseline urban activity; the Discussion section ("Activity-Effect Confound") returns to this distinction.

Fourth, leave-one-cluster-out re-estimation confirms that dropping any single metropolitan cluster (Pyongyang-metro, east-coast, west-coast, or east-inland) leaves the four headline coefficients directionally stable. Leave-one-city-out checks across all sixteen cities show that the PD scarring × PostSanctions coefficient does not flip sign in any of sixteen subsamples; the PD impact × PostCOVID coefficient retains its sign in fourteen of sixteen, with the two exceptions (dropping KNG or RSN) reducing the magnitude.

Fifth, a pre-trend sensitivity check (excluding the top decile of PD events by pre-event NTL elevation; n = 246 of 273 retained) yields directionally identical coefficients with similar magnitudes: PD impact × PostSanctions moves from −0.030 to −0.036; PD impact × PostCOVID from −0.061 to −0.070; PD scarring × PostSanctions from +0.072 to +0.067. The pre-trend therefore does not appear to drive the main coefficients. Figures 5 and 6 visualize the regime contrasts as box plots and the FE coefficients under three baseline definitions, respectively. As a conservative reminder, with only G = 4 metropolitan clusters the exact-enumeration WCB attains a p-value floor of 1/16 ≈ 0.063; headline directional findings remain stable in LOC and LOO checks, but statistical certainty should be interpreted within this small-cluster constraint.

<Figure 5> Pre-sanctions / Post-sanctions / Post-COVID box plots of resilience metrics, computed under the fixed pre-sanctions baseline

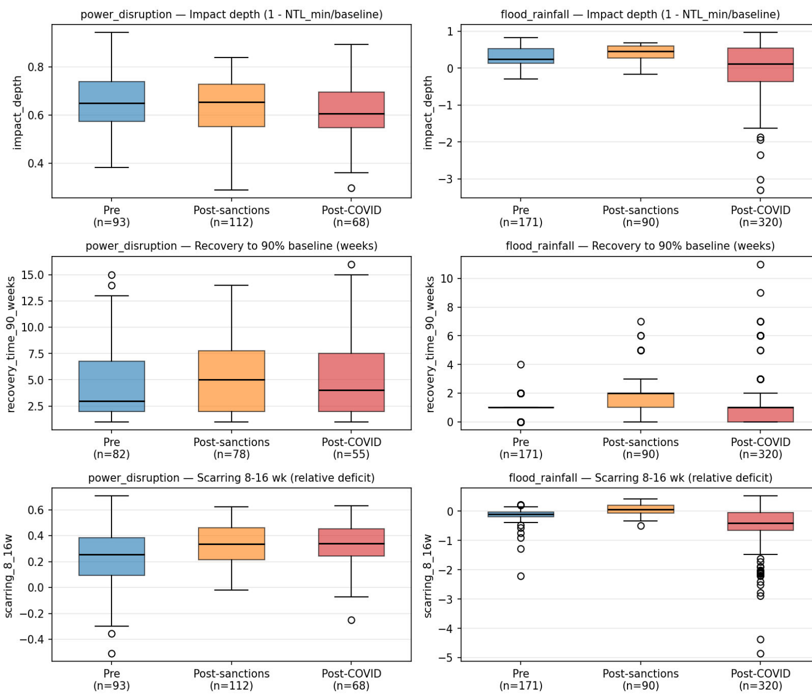

Source: Authors' construction. Power-disruption events appear in the left column; flood-rainfall events in the right column.

<Figure 6> City fixed-effects regression coefficients for PD metrics under three baseline definitions

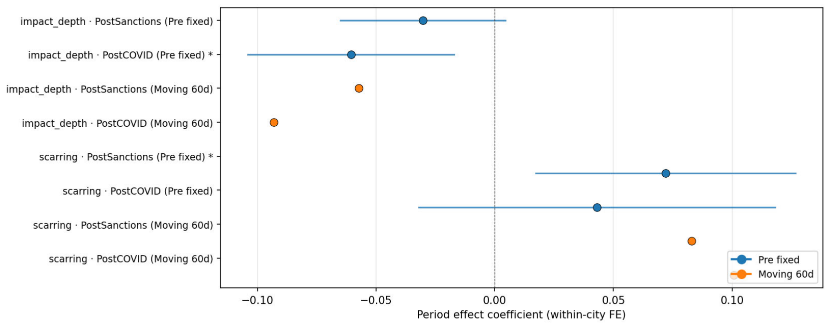

Source: Authors' computations. Coefficient signs and significance patterns are directionally similar across baselines, with attenuated magnitudes under adaptive baselines (moving-median 60-day and week-of-year) that partly absorb the structural NTL decline in the post-period. The attenuation is substantively meaningful: part of the post-COVID effect reflects lower underlying urban activity rather than event-specific disruption.

4. Heterogeneous Treatment Effects (Exploratory)

The heterogeneous-treatment-effect specification reveals a politically counterintuitive pattern under post-COVID conditions (Table 4). These results are reported as exploratory — Table 4 carries HC3-based standard errors only; conservative WCB inference is not applied here because the interaction terms involve subcluster contrasts whose WCB behavior is unstable at G = 4. The PD impact for low-treatment-intensity cities — the political-administrative core — is −0.120 (HC3 $p < 0.001$), substantially deeper than the population-average estimate. The interaction PostCOVID × high reverses this attenuation by +0.073 (HC3 $p = 0.013$) and PostCOVID × medium by +0.067 (HC3 pp = 0.076). In other words, politically protected, low-exposure cities appear to show larger post-COVID PD impacts than high-exposure border and industrial cities, opposite to what a simple exposure-resilience mapping would predict. The pattern is consistent with H3, the hypothesis of "COVID override through prior adaptation"; however, it should be treated as a suggestive direction warranting further investigation rather than as a definitive finding. By contrast, the post-sanctions interactions are not statistically distinguishable from zero, leaving H2 unsupported by the present data. The discussion section interprets the H3 pattern through an “adaptation under sanctions” mechanism.

<Table 4> Heterogeneous treatment effects — PD impact × treatment-intensity interactions

Term	β	SE	p (HC3)
PostSanctions (low ref.)	−0.076	0.066	0.25
PostSanctions × medium	+0.032	0.071	0.65
PostSanctions × high	+0.068	0.074	0.36
PostCOVID (low ref.)	−0.120	0.027	<0.001
PostCOVID × medium	+0.067	0.038	0.076
PostCOVID × high	+0.073	0.029	0.013

Note: City fixed effects are included. n = 273. Low-intensity cities are the reference category. Source: Authors' computations.

5. Hypothesis-Verification Summary

Table 5 summarizes the verification status of the five hypotheses against the empirical evidence above. The H2 verdict ("Not supported") concerns whether the post-sanctions FL response is *disproportionately* larger in high-exposure cities relative to low-exposure cities; the average post-sanctions FL coefficient is positive (Table 3), but the exposure-gradient version of the hypothesis lacks supporting evidence in the heterogeneous-treatment specification.

<Table 5> Hypothesis-verification summary

Hypothesis	Predicted	Evidence	Verdict
H1 — Capital protection	Pyongyang-metro PD frequency < periphery	PD per city-year: 0.69 vs 2.49 (east-inland); illustrative 4-vs-2 ratio 5.6-fold (Table 2)	Supported

H2 — Sanctions exposure (FL impact)	High-exposure cities show larger Post-sanctions FL impact than low-exposure	PostSanctions × high interaction: +0.009 (not significant); FL HTE × intensity does not show systematic ordering by exposure	Not supported
H3 — COVID override through prior adaptation (exploratory)	High-exposure cities show smaller absolute post-COVID PD impact than low-exposure	PostCOVID × high: +0.073 (HC3 p = 0.013, exploratory; no WCB validation), reversing the −0.120 low-exposure baseline (Table 4)	Supported (exploratory)
H4a — Rainfall occurrence physical	FL frequency less politically clustered than PD	FL events 39–46 per FL-eligible city across periods (Figure 4); no political-geographic clustering	Supported
H4b — Rainfall impact may still be political	NTL response to extreme rainfall may vary across cities by political-geographic capacity	Direct test requires ground-truth flood-damage and infrastructure-condition data, which are unavailable for North Korea	Inconclusive

6. Spatial Diagnostics, Pre-Trend, and Robustness Checks

Moran's I on city-level residuals from the fixed-effects regression (inverse-distance weights, 999 permutations) is statistically indistinguishable from zero in all four main specifications (PD impact p = 0.61; PD scarring p = 0.61; FL impact p = 0.49; FL scarring p = 0.16). Spatial autoregressive corrections (SAR or SEM) are not indicated by this diagnostic.

The event-study specification estimating event-time-by-period coefficients shows a V-shaped recovery pattern with a positive overshoot at twelve weeks post-event in the pre-period (+0.14, p < 0.001), dampened in both post-sanctions and post-COVID periods. A joint Wald test on pre-event week dummies yields $\chi^2(7)$ =

16.92, p = 0.018 — a weak but detectable positive pre-trend, strongest at weeks −6 and −5. The analysis offers a detection-mechanism interpretation: PD detection requires a substantial NTL drop, which is more likely to be flagged after periods of slightly elevated activity given a baseline normalized to the long-term mean. This pattern is consistent with a detection-mechanism explanation, but it also cautions against strong causal interpretation of event-time coefficients themselves. The main resilience-metric regressions (Table 3) operate on aggregated post-event recovery characteristics rather than on individual event-time fluctuations, so the pre-trend's impact on those headline coefficients is limited. The pre-trend sensitivity check reported above (excluding the top decile of events by pre-event NTL elevation) shows that the main coefficients remain directionally identical with similar magnitudes after exclusion, further bounding the pre-trend's influence.

V. Discussion

1. The Capital Protection Contrast and Selective State Capacity

The substantial gap in PD frequency between the Pyongyang-metropolitan cluster (0.69 per city-year) and the inland-border periphery (east-inland 2.49 per city-year; east-coast 2.10) is the starkest distributional finding (Table 2). The illustrative four-vs-two-city contrast (17 vs 96 events; 5.6-fold raw or 11-fold by rate) is consistent with this broader pattern rather than driven by selective comparator choice. Two observations strengthen the substantive interpretation. First, Pyongsong (PSG), the second-most luminous city in the sample, records only one PD event in thirteen years, while Kanggye (KNG), an inland city of much lower luminosity, accumulates 58. The difference is especially large between cities of different political-functional categories rather than between cities of different signal strength alone. Second, the broader cluster comparison shows the same ordering — protected core much lower than periphery — across multiple comparison schemes.

The finding is most parsimoniously interpreted through the *selective state capacity* concept (Levitsky & Way, 2010; Wallace, 2014). The pattern is consistent with a system in which scarce electricity, fuel, and maintenance resources are allocated by political function. Pyongyang and its immediate satellites — Pyongsong (administrative-scientific satellite, home to the State Academy of Sciences), Anju and Sunchon (chemical complexes supporting the capital), Sariwon (agriculture-administrative) — receive preferential supply that buffers them against electrical and operational disruptions experienced by the rest of the country. The functional roles of these cities are documented in Park Young-ja (2015) and Min Kyung-Tae (2014). The complement is the heightened vulnerability of the inland-border periphery: Kanggye in Chagang Province hosts military-industrial complexes politically important to the regime but geographically distant from the capital and difficult to supply through the centralized grid; Rason, a special economic zone on the Russian-Chinese tri-border, is similarly remote. Both bear the consequences of selective allocation: PD episodes are frequent because their priority is lower despite their strategic importance. This pattern challenges a simple narrative that authoritarian regimes uniformly protect strategic assets; instead, strategic importance and resource priority operate on different geographic logics, with political-administrative centrality dominating. In the North Korean context, the contrast between H1 (supported) and H2 (not supported) is itself the substantive interpretation: the political-allocation logic that produces the capital-protection contrast operates on cities' political function rather than on their commodity-export exposure, so sanctions-era stress is visible as a centre-periphery PD frequency gap (H1) without producing a clean export-exposure gradient in flood-rainfall NTL response (H2).

2. Adaptation under Sanctions

The most counterintuitive finding is that politically protected low-exposure cities show larger post-COVID PD impacts than high-exposure border and industrial cities. A simple exposure-resilience mapping would predict the opposite. An adaptation-under-sanctions mechanism reconciles the result. Between 2017 and

2019, high-exposure cities experienced a direct contraction of their primary economic activities — coal exports through Chongjin and Kimchaek, cross-border trade through Sinuiju, mineral exports — and had three years to adjust downward, reorganize internal supply chains, and stabilize at a new lower equilibrium (Lee Suk, 2021). By 2020, when COVID-19 closed the border completely, these cities had limited residual cross-border activity left to lose. Politically protected cities followed a different trajectory: through 2017–2019, resources were prioritized to Pyongyang and its satellites, maintaining urban activity near pre-sanctions levels. This required cross-border flows — fuel imports through Nampo and Sinuiju, food and equipment imports — channeled disproportionately to the capital region. When the 2020 border closure cut off these flows, the priority allocation system itself lost its primary inputs. Protected cities experienced larger relative drops because they had been operating closer to pre-sanctions baselines.

Two implications follow: (i) resilience is a function of adaptation history, with previously adapted cities paradoxically more robust to subsequent shocks; and (ii) compound external shocks disrupt not only economic flows but also the political-economic allocation system that buffered cities differentially.

3. The Activity-Effect Confound — Applied Consistently

The FL results may appear contradictory if interpreted as straightforward resilience changes. They instead reflect different combinations of two phenomena. In the post-sanctions period, NTL losses following extreme rainfall events became larger. This pattern is consistent with weakened drainage or response capacity (OCHA, 2019; Smith, 2015; Lee Suk, 2021), but the present data do not directly observe inundation, physical damage, or infrastructure condition; baseline urban activity itself may also have declined between 2012–2015 and 2017–2019, so part of the FL post-sanctions effect may reflect baseline-activity changes rather than infrastructure deterioration. Under post-COVID, the physical infrastructure did not improve; rather, urban *activity* — the lights that constitute the NTL measurement — contracted dramatically due to industrial slowdown and pandemic-related operational disruptions. With lower baseline NTL, a given physical flooding event produces a smaller proportional anomaly. The moving-window baseline produces attenuated estimates relative to the fixed pre-sanctions baseline (see Figure 5 caption), consistent with the activity-effect interpretation. This activity-effect confound is a known challenge in satellite-NTL resilience analysis (Elvidge et al., 2020; Henderson et al., 2018), and this paper applies it consistently to both post-sanctions and post-COVID coefficients: any inference about underlying infrastructural resilience must be tempered by the recognition that baseline activity itself shifted across regimes. A complete decomposition would require independent measurement of urban activity, which is not feasible for North Korea. A related caveat applies to the post-COVID period: in cities whose baseline urban activity was already depressed before 2020, the *incremental* NTL signature of an additional power-disruption or flood event may be small relative to the noise floor of the satellite measurement, so part of what appears as “diminished impact” after 2020 may reflect the limit of NTL sensitivity at low baseline activity rather than genuine resilience.

4. Limitations

Five limitations qualify the findings. First, without ground-truth electricity records or flood-impact data for North Korea, external validation remains unavailable; the placebo and control-ring tests provide internal validation only. Second, sixteen cities still represent only a fraction of the country's urban centers with populations above 100,000, and three (HYS, SCN, KNG) are further excluded from FL analysis under the terrain-risk filter defined before model estimation. Third, the metropolitan-cluster count ($G = 4$) is small for cluster-robust inference; the exact-enumeration WCB partially addresses this but cannot eliminate the floor on attainable p-values. Fourth, the detection algorithm produces a weak positive pre-trend, interpreted as a detection artifact and bounded in influence by the pre-trend sensitivity check (see Results). Fifth, the analysis cannot definitively separate sanctions effects from other 2017–2025 factors (diplomatic shifts of 2018–2019, internal political developments, weather variation), a long-standing limitation of quasi-observational work on North Korea.

Seasonal data availability also affects interpretation: the asymmetry between the high-FL-risk season (summer, high data availability) and the high-PD-risk season (winter, lower data availability) introduced in the Data section means PD detection is comparatively constrained in the season of highest underlying disruption risk.

5. Ethical Considerations

Satellite-derived data on closed states should not be used to refine sanctions enforcement against civilian-affecting targets or for surveillance objectives that would compound humanitarian harm. The present paper's contribution lies in opening evidentiary space for academic and humanitarian inquiry; appropriate institutional safeguards for downstream uses are warranted. In particular, the city-level patterns documented here — most notably the capital-protection contrast — should inform humanitarian targeting and academic discussion rather than coercive policy. Researchers conducting future remote-sensing work on opaque states are encouraged to consider similar restraint in framing, dissemination, and data-sharing practices.

Ⅵ. Conclusion

The observed urban consequences of international sanctions and the pandemic-era border closure were unevenly distributed across North Korea's political geography. A substantial capital-protection contrast emerges in power-disruption frequency between the Pyongyang-metropolitan core and the inland-border periphery; NTL responses to flood-inducing rainfall became larger during the post-sanctions period; and the post-COVID period produces a counterintuitive heterogeneous-treatment-effect pattern in which politically protected cities show larger NTL impacts than high-exposure cities — consistent with an “adaptation under sanctions” mechanism.

These findings support and extend the literatures on authoritarian urban politics, selective state capacity, and the within-country distributional consequences of sanctions, and they are positioned alongside the Korean-language scholarship of Park Young-ja, Lee Suk, Kim Byung-Yeon, Yang Moon-Soo, and Min Kyung-Tae on North Korean urban political economy.

The paper's methodological contribution expands the evidentiary repertoire available for research on closed or data-poor states: daily satellite nighttime-lights data, combined with transparent event definitions, fixed-effects panel inference, and conservative reporting with small numbers of clusters, can produce credible cross-city evidence where survey and administrative data are unavailable. The methodological possibility extends beyond the North Korean case to other sanctioned authoritarian states and to natural-disaster political-economy analysis in contexts where official statistics are weak, suggesting that satellite-derived measures deserve broader use in Korean studies and comparative political economy as a complement — not a substitute — for qualitative and survey-based work.

Future extensions include integration of higher-resolution precipitation data for finer flood detection, climate-reanalysis integration for cold-wave compound events, expansion to additional North Korean cities under alternative detection thresholds, cross-country comparison with other sanctioned authoritarian states, and detrended-baseline robustness specifications.

Policy implications. The capital-protection contrast suggests that humanitarian assistance distributed through capital-region channels — the easiest delivery routes for international aid agencies — may systematically under-reach the peripheral cities (Kanggye, Rason, Hyesan, and other east-inland and east-coast industrial centers) where urban disruption is empirically most frequent; aid targeting should therefore include direct peripheral-city support where politically feasible. The observed post-sanctions deterioration of FL resilience further indicates that humanitarian flood-response planning should treat compound climate-and-sanctions shocks together rather than as separate risk channels. The exploratory adaptation-under-sanctions pattern, if confirmed in subsequent work, suggests that compound external shocks differ qualitatively from either shock alone, with implications for the sanctions-design debate about the distributional incidence of pressure on regime versus civilian populations.

Acknowledgments

During the preparation of figures and tables for this manuscript, the authors used Claude Code (Anthropic, Opus 4.7) to assist with the editing and formatting of data and result visualizations (matplotlib figure script revisions for readability, Word document layout adjustments, and table-formatting cleanup). The underlying data, analytical results, and interpretive content are the authors' own; the AI assistant was not used to generate research findings or original written argument.

참고문헌

Allen, Susan Hannah. (2008). Political Institutions and Constrained Response to Economic Sanctions. Foreign *Policy Analysis* 4(3), 255–274. https://doi.org/10.1111/j.1743-8594.2008.00069.x

Bruneau, Michel, Chang, Stephanie E., Eguchi, Ronald T., Lee, George C., O'Rourke, Thomas D., Reinhorn, Andrei M., Shinozuka, Masanobu, Tierney, Kathleen, Wallace, William A., & von Winterfeldt, Detlof. (2003). A Framework to Quantitatively Assess and Enhance the Seismic Resilience of Communities. *Earthquake Spectra* 19(4), 733–752. https://doi.org/10.1193/1.1623497

Cameron, A. Colin, Gelbach, Jonah B., & Miller, Douglas L. (2008). Bootstrap-Based Improvements for Inference with Clustered Errors. *Review of Economics and Statistic*s 90(3), 414–427. https://doi.org/10.1162/rest.90.3.414

Cohen, Charles & Werker, Eric D. (2008). The Political Economy of "Natural" Disasters. *Journal of Conflict Resolution* 52(6), 795–819. https://doi.org/10.1177/0022002708322157

Drezner, Daniel W. (1999). *The Sanctions Paradox: Economic Statecraft and International Relations*. Cambridge: Cambridge University Press.

Early, Bryan R. (2015). *Busted Sanctions: Explaining Why Economic Sanctions Fail*. Stanford, CA: Stanford University Press.

Elvidge, Christopher D., Baugh, Kimberly, Zhizhin, Mikhail, Hsu, Feng-Chi, & Ghosh, Tilottama. (2017). VIIRS Night-Time Lights. *International Journal of Remote Sensing* 38(21), 5860–5879. https://doi.org/10.1080/01431161.2017.1342050

Elvidge, Christopher D., Zhizhin, Mikhail, Ghosh, Tilottama, Hsu, Feng-Chi, & Taneja, Jay. (2020). Indicators of Electric Power Instability from Satellite Observed Nighttime Lights. *Remote Sensing* 12(19), 3194. https://doi.org/10.3390/rs12193194

Funk, Chris, Peterson, Pete, Landsfeld, Martin, Pedreros, Diego, Verdin, James, Shukla, Shraddhanand, Husak, Gregory, Rowland, James, Harrison, Laura, Hoell, Andrew, & Michaelsen, Joel. (2015). The Climate Hazards Infrared Precipitation with Stations: A New Environmental Record for Monitoring Extremes. *Scientific Data* 2, 150066. https://doi.org/10.1038/sdata.2015.66

GADM. (2022). *GADM Database of Global Administrative Areas* (Version 4.1). https://gadm.org/ (Accessed: March 18, 2026).

Geofabrik. (2024). *OpenStreetMap Data Extracts*. © OpenStreetMap contributors, ODbL 1.0. https://download.geofabrik.de/ (Accessed: March 18, 2026).

Gillies, Sean. (2013-present). *Rasterio: Geospatial Raster I/O for Python Programmers*. https://github.com/rasterio/rasterio (Accessed: March 18, 2026).

Haggard, Stephan & Noland, Marcus. (2017). *Hard Target: Sanctions, Inducements, and the Case of North Korea*. Stanford, CA: Stanford University Press.

Henderson, J. Vernon, Squires, Tim, Storeygard, Adam, & Weil, David N. (2018). The Global

Distribution of Economic Activity: Nature, History, and the Role of Trade. *Quarterly Journal of Economics* 133(1), 357–406. https://doi.org/10.1093/qje/qjx030

Henderson, J. Vernon, Storeygard, Adam, & Weil, David N. (2012). Measuring Economic Growth from Outer Space. *American Economic Review* 102(2), 994–1028. https://doi.org/10.1257/aer.102.2.994

Hodler, Roland & Raschky, Paul A. (2014). Regional Favoritism. *Quarterly Journal of Economics* 129(2), 995–1033. https://doi.org/10.1093/qje/qju004

Hoyer, Stephan & Hamman, Joseph. (2017). xarray: N-D Labeled Arrays and Datasets in Python. *Journal of Open Research Software* 5(1), 10. https://doi.org/10.5334/jors.148

Hufbauer, Gary Clyde, Schott, Jeffrey J., Elliott, Kimberly Ann, & Oegg, Barbara. (2007). *Economic Sanctions Reconsidered* (3rd ed.). Washington, DC: Peterson Institute for International Economics.

Jordahl, Kelsey, Van den Bossche, Joris, Fleischmann, Martin, Wasserman, Jacob, McBride, James, Gerard, Jeffrey, Tratner, Jeff, Perry, Matthew, Badaracco, Adrian Garcia, Farmer, Carson, Hjelle, Geir Arne, Snow, Alan D., Cochran, Micah, Gillies, Sean, Culbertson, Lucas, Bartos, Matt, Eubank, Nick, Bilogur, Aleksey, & Leblanc, Frederick. (2020). *geopandas/geopandas: v0.7.0* [Software]. Zenodo.

Kim Byung-Ro [김병로]. (2012). 북한의 분절화된 시장화와 정치사회적 함의 [North Korea's Segmented Marketization and Its Politico-Social Implications]. *북한연구학회보 [North Korean Studies Review]* 16(1).

Kim Byung-Yeon. (2017). Unveiling the North Korean Economy: Collapse and Transition. Cambridge: Cambridge University Press.

Lankov, Andrei. (2013). *The Real North Korea: Life and Politics in the Failed Stalinist Utopia*. New York, NY: Oxford University Press.

Lee Suk [이석]. (2021). *대북제재의 영향력과 북한의 경제적 미래 [The Impact of DPRK Sanctions and North Korea's Economic Future]* (KDI Research Monograph 2021-01). Sejong: Korea Development Institute.

Lee Yong Suk. (2018). International Isolation and Regional Inequality: Evidence from Sanctions on North Korea. *Journal of Urban Economics* 103, 34–51. https://doi.org/10.1016/j.jue.2017.11.002

Levitsky, Steven & Way, Lucan A. (2010). *Competitive Authoritarianism: Hybrid Regimes after the Cold War*. Cambridge: Cambridge University Press.

Meerow, Sara, Newell, Joshua P., & Stults, Melissa. (2016). Defining Urban Resilience: A Review. *Landscape and Urban Planning* 147, 38–49. https://doi.org/10.1016/j.landurbplan.2015.11.011

Min Kyung-Tae [민경태]. (2014). *서울 평양 메가시티 [Seoul-Pyongyang Mega-City]*. Seoul: Mirae-ui-chang.

NASA JPL. (2013). *NASA Shuttle Radar Topography Mission Global 1 Arc Second* (SRTMGL1, V003)

[Data set]. NASA EOSDIS Land Processes DAAC. https://doi.org/10.5067/MEaSUREs/SRTM/SRTMGL1.003

Neuenkirch, Matthias & Neumeier, Florian. (2015). The Impact of UN and US Economic Sanctions on GDP Growth. *European Journal of Political Economy* 40(A), 110–125. https://doi.org/10.1016/j.ejpoleco.2015.09.001

OCHA. (2019). *2019 DPR Korea Needs and Priorities*. New York: United Nations Office for the Coordination of Humanitarian Affairs. https://reliefweb.int/report/democratic-peoples-republic-korea/2019-dpr-korea-needs-and-priorities (Accessed: March 18, 2026).

Pape, Robert A. (1997). Why Economic Sanctions Do Not Work. *International Security* 22(2), 90–136. https://doi.org/10.1162/isec.22.2.90

Park Young-ja [박영자]. (2015). *북한의 시장화와 정치사회 균열 [North Korea's Marketization and Politico-Social Cleavages]*. Seoul: Korea Institute for National Unification.

Park Y. (2022). *Efficacy of Economic Sanctions against North Korea: Evidence from Satellite Nighttime Lights* (KIEP World Economy Brief No. 22-03). Sejong: Korea Institute for International Economic Policy.

Peksen, Dursun. (2009). Better or Worse? The Effect of Economic Sanctions on Human Rights. *Journal of Peace Research* 46(1), 59–77. https://doi.org/10.1177/0022343308098404

Román, Miguel O., Stokes, Eleanor C., Shrestha, Ranjay, Wang, Zhuosen, Schultz, Lori, Sepúlveda Carlo, Edil A., Sun, Qingsong, Bell, Jordan, Molthan, Andrew, Kalb, Virginia, Ji, Chuanyi, Seto, Karen C., McClain, Shanna N., & Enenkel, Markus. (2019). Satellite-Based Assessment of Electricity Restoration Efforts in Puerto Rico after Hurricane Maria. *PLOS ONE* 14(6), e0218883. https://doi.org/10.1371/journal.pone.0218883

Román, Miguel O., Wang, Zhuosen, Sun, Qingsong, Kalb, Virginia, Miller, Steven D., Molthan, Andrew, Schultz, Lori, Bell, Jordan, Stokes, Eleanor C., Pandey, Bhartendu, Seto, Karen C., et al. (2018). NASA's Black Marble Nighttime Lights Product Suite. *Remote Sensing of Environment* 210, 113–143. https://doi.org/10.1016/j.rse.2018.03.017

Seabold, Skipper & Perktold, Josef. (2010). Statsmodels: Econometric and Statistical Modeling with Python. In *Proceedings of the 9th Python in Science Conference*, 92–96. https://doi.org/10.25080/Majora-92bf1922-011

Slater, Dan. (2010). *Ordering Power: Contentious Politics and Authoritarian Leviathans in Southeast Asia*. Cambridge: Cambridge University Press.

Smith, Hazel. (2015). *North Korea: Markets and Military Rule*. Cambridge: Cambridge University Press.

Tierney, Kathleen. (2014). *The Social Roots of Risk: Producing Disasters, Promoting Resilience*. Stanford, CA: Stanford University Press.

Wallace, Jeremy L. (2014). *Cities and Stability: Urbanization, Redistribution, and Regime Survival in China*. New York, NY: Oxford University Press.

Wang, Zhuosen, Román, Miguel O., Kalb, Virginia L., Miller, Steven D., Zhang, Jianglong, & Shrestha, Ranjay M. (2021). Quantifying Uncertainties in Nighttime Light Retrievals from Suomi-NPP and NOAA-20 VIIRS Day/Night Band Data. *Remote Sensing of Environment* 263, 112557. https://doi.org/10.1016/j.rse.2021.112557

Yang Moon-Soo [양문수]. (2005). 북한에서의 시장의 형성과 발전: 생산물시장을 중심으로 [Formation and Development of Markets in North Korea: Focusing on Product Markets]. *비교경제연구 [Comparative Economic Studies]* 12(2).

Manuscript: May 22, 2026; Review completed: June 09, 2026;
Accepted: June 15, 2026